ELSEVIER

Influence of textural and wettability variations on predictions of DNAPL persistence and plume development in saturated porous media

Thomas J. Phelan [a,1], Lawrence D. Lemke [a,1], Scott A. Bradford [b,2],
Denis M. O'Carroll [a,1], Linda M. Abriola [c,*]

[a] *Department of Civil and Environmental Engineering, University of Michigan, 181 EWRE, 1351 Beal Ave., Ann Arbor, MI 48109-2125, USA*
[b] *George E. Brown, Jr. Salinity Laboratory, US Department of Agriculture, Agricultural Research Service,
450 Big Springs Rd., Riverside, CA 92507, USA*
[c] *School of Engineering, Tufts University, 105 Anderson Hall, 200 College Ave., Medford, MA 02155, USA*

Abstract

Numerical simulations examine the migration, entrapment, and mass recovery behavior of DNAPLs in aquifer systems with coupled textural and wettability variations. Permeability fields of varying degrees of heterogeneity (i.e., differing $\sigma^2_{\ln(k)}$) were generated with sequential Gaussian simulation, using geostatistical parameters derived from core grain size measurements in a sandy glacial outwash aquifer. Organic-wet mass fraction, a representative metric for wettability, was correlated to porous media permeability. A multiphase flow simulator incorporating wettability-dependent constitutive relationships for capillary behavior is used to generate residual saturation distributions for tetrachloroethene (PCE) spill events in these synthetic aquifers. Simulated saturation distributions then serve as initial conditions for compositional simulations of PCE dissolution, to examine the effect of coupled wettability and permeability variations on DNAPL mass recovery. Simulations reveal considerable differences in predicted depth of organic liquid penetration, extent of vertical spreading, and magnitude of maximum entrapped saturation for the various modeled scenarios. These differences are directly linked to observable variations in effluent concentration and mass recovery predictions in the aqueous phase flushing simulations. Results suggest that mass recovery behavior may be highly realization dependent and not closely correlated with geostatistical parameters.
© 2004 Elsevier Ltd. All rights reserved.

Keywords: Multiphase flow; DNAPL; Wettability; Heterogeneity; Numerical model; Source zone remediation

1. Introduction

The accidental or intentional introduction of low solubility organic compounds into the subsurface has led to widespread contamination of groundwater resources. These contaminants are often released as a separate, immiscible phase known as a nonaqueous phase liquid (NAPL). Of particular concern is the behavior of dense nonaqueous phase liquids (DNAPLs), which migrate through the vadose and saturated zones under gravitational and pressure forces, leaving behind pooled or entrapped residual organic liquid mass [52,75]. This pooled and entrapped organic liquid has the potential to contaminate significant volumes of groundwater over lengthy time scales due to its low aqueous phase solubility.

The fate and transport of DNAPL contaminants is known to be controlled by spatial heterogeneity in physical and chemical properties. Numerical [13,24, 30,43,47], laboratory [75], and field [55] studies have examined the effect of spatial variability in physical properties on the flow and entrapment of immiscible liquids in the saturated zone. Other studies have investigated the effect of spatial variability on source zone

* Corresponding author. Fax: +1-617-627-3819.
E-mail addresses: tphelan@engin.umich.edu (T.J. Phelan), ldlemke@engin.umich.edu (L.D. Lemke), sbradford@ussl.ars.usda.gov (S.A. Bradford), denismo@engin.umich.edu (D.M. O'Carroll), linda.abriola@tufts.edu (L.M. Abriola).
[1] Fax: +1-734-763-2275.
[2] Fax: +1-909-342-4963.

remediation and mass flux of contaminant dissolved in the aqueous phase [21,25,32,36,46,66,67,69].

A common assumption in these investigations is that the porous media are completely water-wet. In water-wet media, water preferentially coats the solid surface. In systems where both water and an organic liquid are present, the water will be retained in the small pores/finer textured material and the organic liquid will reside in the larger pore spaces/coarser textured material. Wettability influences both capillary pressure–saturation [5] and relative permeability [6] relationships and will have a significant effect on the overall distribution of DNAPL in the subsurface.

Since most uncontaminated aquifer materials (especially those that are quartz-based) are strongly water-wetting, it has been typically assumed that this is also the case when the material is contaminated. However, a number of laboratory investigations in the petroleum recovery and hydrology literature have demonstrated that solid phase wettability can vary with a variety of factors, such as: solid phase mineralogy [4], surface roughness [53], pH [50], presence of organic acids and bases [29,50,64,65,70,77], exposure to coal tar [56,73], exposure to synthetic gasolines [57], and exposure to surface active solutes [33,38]. Of particular concern is the fact that many DNAPLs used in degreasing and dry-cleaning operations (e.g., chlorinated solvents) may contain surface active additives.

A number of studies have been undertaken to examine multiphase fluid behavior in formations exhibiting spatial variability in physical properties (permeability, porosity, and capillary parameters) [24,31,43,44,60]. These studies have shown that the spatial distribution of multiphase flow parameters has an observable influence on predictions of organic liquid migration pathways and entrapment volumes. These conclusions are supported by several laboratory [8,37,74] and field scale [30,45] observations.

Comparatively little work has been undertaken to examine the effect of solid phase wettability on predictions of DNAPL migration, entrapment, and mass removal. The limited investigations suggest that increasing amounts of organic-wet material are associated with higher maximum organic liquid saturations and decreased depths of penetration [13]. The presence of organic-wet capillary barriers has also been shown to strongly affect both the entrapment and dissolution of organic liquids in laboratory sand tank experiments [18].

This paper extends previous investigations [13] of DNAPLs in coupled physically and chemically heterogeneous porous media. This investigation [13] was based upon a very limited and somewhat hypothetical set of permeability realizations. By employing a larger ensemble (three different conditioned realizations and three different levels of physical heterogeneity) of field site-based porous media migration and entrapment

behavior will be systematically examined here. In addition, the effect of these coupled porous media properties on aqueous phase DNAPL-component recovery will also be addressed. The comprehensive modeling framework, incorporating the effect of solid phase wettability, upon which these simulations are based, is first described below.

2. Mathematical model

2.1. Governing equations

A combined mass and momentum balance equation which governs the flow of a fluid phase (α = a (aqueous) or o (organic)) in a porous medium may be written as: [1]

$$\frac{\partial}{\partial t}(\phi \rho_\alpha S_\alpha) = \nabla \cdot \left[\rho_\alpha \frac{\mathbf{k} k_{r\alpha}}{\mu_\alpha}(\nabla P_\alpha - \rho_\alpha \mathbf{g}) \right] + E_{\alpha\beta} + Q_\alpha \quad (1)$$

where ϕ is porosity [–], ρ_α is the α-phase mass density [M/L^3], S_α is the α-phase saturation, $\mathbf{k}$ is the intrinsic permeability tensor [L^2], $k_{r\alpha}$ is the α-phase relative permeability [–], μ_α is the α-phase kinematic viscosity [M/L/T], P_α is the α-phase pressure [M/L/T^2], $\mathbf{g}$ is the gravitational acceleration vector [L/T^2], $E_{\alpha\beta}$ is an interphase mass exchange term between the α- and β-phases [M/L^3/T], and Q_α is an external source or sink to the α-phase [M/L^3/T]. For a two-phase system, additional constitutive relationships (in this case, capillary property relationships) are necessary to close the problem. In addition, mass conservation requires that $\Sigma S_\alpha = 1$.

A component mass balance equation which governs the transport of an aqueous phase component may be written as: [1]

$$\frac{\partial}{\partial t}(\phi S_a \rho^a \chi_i) + \nabla \cdot [\phi S_a (\mathbf{v}_a \rho^a \chi_i - \rho^a \mathbf{D}_h \cdot \nabla \chi_i)t] = E_{oa} \quad (2)$$

where χ_i is the mole fraction of the aqueous phase component i [–], ρ^a is the aqueous phase molar density [mol/L^3], $\mathbf{v}_a$ is the pore velocity of the aqueous phase [L/T], and $\mathbf{D}_h$ is the hydrodynamic dispersion tensor [L^2/T]. Herein, local hydrodynamic dispersion is assumed to be a Fickian process and is evaluated with a traditional groundwater modeling approach [9]. E_{oa}, the interphase mass exchange of the organic component between the DNAPL and aqueous phases, is modeled using a standard linear driving force expression:

$$E_{oa} = \rho^a \hat{k}_l^{oa}(\chi_{eq} - \chi_i) \quad (3)$$

Here, $\hat{k}_l^{ao}$ is a lumped liquid film mass transfer coefficient [T^{-1}] and χ_{eq} represents the equilibrium mole fraction of component i [–] in the aqueous phase. As the emphasis of this study is the investigation of DNAPL mass recovery, organic sorption/desorption to the solid phase will not be considered.

2.2. Wettability-dependent constitutive relationships

There are several common parameterizations of the capillary pressure–saturation (e.g., [20,72]) and relative permeability–saturation (e.g., [22,54]) relationships for water-wet media. These parametric forms must be modified for porous media that possess fractional wettability. Fractional wettability arises when both water-wet and organic-wet surfaces occur within the same representative elementary volume of the porous medium. These modified constitutive relationships should appropriately account for the effect of pore scale wettability variations at the continuum scale. Several wettability-dependent comprehensive capillary pressure–saturation–relative permeability models have been presented in the literature [12,14–16,48,71]. In fractionally-wet porous media, it is possible to have negative capillary pressures (assuming the $P_c = P_o - P_a$ convention) due to the presence of strongly hydrophobic material. Thus, a reference water-wet capillary pressure—saturation curve can be thought of as being "shifted" along the capillary pressure axis. A general capillary pressure—saturation relation may be presented as [15]:

$$P_c\left(\overline{\overline{S_a}}\right) = \sqrt{\frac{k_{ref}}{k}\frac{\phi}{\phi_{ref}}}P_c^{ref}\left(\overline{\overline{S_a}}\right) - \Lambda_{ref} \qquad (4)$$

where k_{ref} [L^2] and ϕ_{ref} [–] are the permeability and porosity of the reference material, $\overline{\overline{S_a}}$ is the apparent water saturation [–], and Λ_{ref} is a shifting parameter [M/L/T^2]. The leading coefficient multiplying the first term of the right-hand side of (4) is a standard Leverett scaling factor [49]. Here, the apparent water saturation ($\overline{\overline{S_a}}$) is defined as [13]:

$$\overline{\overline{S_a}} = \overline{S_a} + \overline{S_{ot}} - \overline{S_{at}} \qquad (5)$$

where $\overline{S_a}$ is the effective aqueous phase saturation $\left(\overline{S_a} = \frac{S_a - S_{ra}}{1 - S_{ra}}\right)$, S_{ra} is the residual aqueous phase saturation, $\overline{S_{ot}}$ is the effective entrapped organic liquid saturation, and $\overline{S_{at}}$ is the effective entrapped aqueous phase saturation. $P_c^{ref}\left(\overline{\overline{S_a}}\right)$ is any particular chosen parameterization of the water-wet capillary pressure–saturation relationship (e.g., [20,72]). In this work, a shifted Brooks and Corey [20] parameterization will be employed:

$$P_c^{ref}\left(\overline{\overline{S_a}}\right) = P_d\overline{\overline{S_a}}^{1/\lambda} \qquad (6)$$

where P_d is the entry pressure [M/L/T^2] and λ is a pore-size distribution parameter [–]. The shifting factor, Λ_{ref}, has been found to depend upon the organic-wet mass fraction and the whether the aqueous phase is undergoing drainage or imbibition. Bradford and Leij [16] used laboratory observations to develop the following correlation for Λ_{ref}:

$$\Lambda_{ref}^D(F_o) = P_{c,\overline{\overline{S_a}}=0.5}^{ref}(a^D F_o + b^D)\rho_a\|\mathbf{g}\| \qquad (7)$$

Table 1
Capillary pressure curve shifting parameters

a^D	7.618×10^{-5} m/Pa
b^D	1.215×10^{-5} m/Pa
a^I	1.554×10^{-4} m/Pa
b^I	6.660×10^{-6} m/Pa

$$\Lambda_{ref}^I(F_o) = P_{c,\overline{\overline{S_a}}=0.5}^{ref}(a^I F_o + b^I)\rho_a\|\mathbf{g}\| \qquad (8)$$

Here, F_o is the mass fraction of organic-wet sand [–], $P_{c,\overline{\overline{S_a}}=0.5}^{ref}$ is the water-wet capillary pressure corresponding to an apparent water saturation of 0.5 [M/L/T^2], and a^D, b^D, a^I, and b^I are fitting parameters [L^{2}T^2/M]. Values for these parameters for selected quartz sands are summarized in Table 1.

Several authors have developed models that predict relative permeability as a function of material wettability [12,39,42,48,51,71] in fractionally-wet unsaturated systems as well as mixed-wet (systems where small pores are water-wet and larger pores are intermediate- to organic-wet) NAPL/water systems. The model used here is an extension of the Burdine [22] relative permeability model for fractionally wet media [12]:

$$k_{rw}\left(\overline{\overline{S_a}}\right) = (\overline{S_a} - \overline{S_{at}})^2$$
$$\times \frac{[1 + \cos(\theta)]\int_0^{\overline{\overline{S_a}}} R(S)^2\,\mathrm{d}S + [1 - \cos(\theta)]\int_{1-\overline{\overline{S_a}}}^1 R(S)^2\,\mathrm{d}S}{2\int_0^1 R(S)^2\,\mathrm{d}S}$$

$$k_{ro}\left(\overline{\overline{S_o}}\right) = (\overline{S_o} - \overline{S_{ot}})^2$$
$$\times \frac{[1 - \cos(\theta)]\int_0^{\overline{\overline{S_o}}} R(S)^2\,\mathrm{d}S + [1 + \cos(\theta)]\int_{1-\overline{\overline{S_o}}}^1 R(S)^2\,\mathrm{d}S}{2\int_0^1 R(S)^2\,\mathrm{d}S}$$
$$(9)$$

Here, $R(S)$ is the pore radius distribution ($R(S) = P_c(S)/2\gamma$, where γ is interfacial tension [M/T^2]) and θ is an effective macroscopic contact angle. As θ nears 0° the porous media behaves as a water-wet media and as θ nears 180° it behaves as an organic-wet media.

Solid phase wettability has been shown to have an observable effect on tetrachloroethene (PCE) dissolution rates in laboratory sand columns [19]. Systems with a high fraction of organic-wet sand exhibit increased rates of interphase mass transfer compared to systems with little or no organic-wet sand. This has been attributed to the existence of films of residual organic liquid in organic-wet sands, in contrast to pore-body ganglia in water-wet sands. Organic liquid configured as a film has a much higher interfacial area and a correspondingly higher interphase mass transfer rate [19]. This investigation employed an empirically-based Sherwood number relationship that correlates lumped film mass transfer coefficients to several experimentally obtainable physicochemical quantities [17]:

$$\mathbb{N}_{\text{Sh}} = 0.254 \left(\frac{d_{50}}{0.05 \text{ cm}} \right)^{0.475} U_i^{-1.187}$$

$$\times \mathbb{N}_{\text{Re}}^{0.654} \mathbb{N}_{\text{Sc}}^{0.486} \left(\frac{S_{\text{o}}}{S_{\text{o}}^{\text{init}}} \right)^{0.959(1-F_{\text{o}})\frac{6.265}{U_i}} \quad (10)$$

Here, $\mathbb{N}_{\text{Sh}}$ is the Sherwood number $\left(\mathbb{N}_{\text{Sh}} = \frac{\hat{k}_l^{\text{ao}} d_{50}^2}{D_{\text{m}}} \right)$, d_{50} is the mean grain diameter [L], D_{m} is the free liquid diffusivity [L^2/T], U_i is the uniformity index [–], $\mathbb{N}_{\text{Re}}$ is the Reynolds number $\left(\mathbb{N}_{\text{Re}} = \frac{\rho_{\text{a}} \|\mathbf{v}_{\text{a}}\| d_{50}}{\mu_{\text{a}}} \right)$, $\mathbb{N}_{\text{Sc}}$ is the Schmidt number $\left(\mathbb{N}_{\text{Sc}} = \frac{\mu_{\text{a}}}{\rho_{\text{a}} D_{\text{m}}} \right)$, and $S_{\text{o}}^{\text{init}}$ is the initial entrapped organic liquid saturation.

2.3. Numerical implementation

The wettability-dependent capillary property model (Eqs. (4),(7)–(10)) was incorporated in an extensively modified version of the VALOR model [3] known as M-VALOR. M-VALOR is a block-centered finite difference code capable of solving the fully coupled multiphase flow equations for three mobile phases (aqueous, gas, and DNAPL). It uses an iterative implicit pressure-explicit saturation (IMPES) scheme to solve the linearized system of continuum equations (Eq. (1)). M-VALOR has been shown to be a robust, computationally efficient code for the simulation of a variety of multiphase flow problems [13,24,26,59–61].

The wettability-dependent interphase mass transfer model (10) was incorporated into a modified version of MISER, a compositional flow and transport simulator originally designed [63] to model soil vapor extraction and bioventing scenarios. MISER solves flow and transport equations (1) and (2) using a standard Galerkin finite element method employing linear basis functions on triangular elements. Nonlinearities are handled using a quasi-Newton iteration. Single valued nodal phase velocities are obtained through a Galerkin finite element solution of Darcy's Law. In addition, to fully account for spatial discontinuities in saturation, mobility, and interphase mass exchange MISER maintains and numerically tracks discontinuous variables at material property interfaces [2]. MISER has been shown to be mathematically accurate via global mass balance calculations, comparisons with one- and two-dimensional analytical solutions, as well as comparisons with other numerical models [63]. Recently, MISER has been successfully used to model laboratory-scale aquifer remediation experiments in nonuniform media [62].

3. Model application

The modified models, M-VALOR and MISER, were used to numerically investigate the effect of coupled physical and chemical spatial heterogeneity on estimates of DNAPL entrapment and mass recovery. The computational domain was selected based upon a PCE spill scenario investigated by Lemke et al. [47] for a contaminated unconfined glacial outwash formation in Oscoda, Michigan. PCE was chosen as the representative DNAPL for this study (cf. PCE properties in Table 2). PCE was introduced into the top of the domain over a region 1.22 m wide at a rate of 0.240 l/day. The PCE was allowed to infiltrate for a period of 400 days, followed by a 330 day period of organic liquid redistribution. At this point the PCE had ceased to flow under gravitational, viscous, and capillary forces. These values for spill size and release rate were chosen to be consistent with a slow PCE leak over an extended period of time, similar to that which occurred at the former dry cleaner in Oscoda.

The aquifer at this site consists of relatively homogeneous medium-fine sand underlain by a thick clay layer 8.00 m below grade. Heterogeneous fields of d_{10} values were generated using conditional sequential Gaussian simulation, with distribution parameters (cf. Table 3) based on a geostatistical analysis of 167 site core samples. Sequential Gaussian simulation assumes a Gaussian random function distribution for the variable of interest (in this case, the distribution of d_{10} values). This allows the univariate distribution to be completely described by its mean and variance. In addition, definition of the bivariate distribution requires only a semivariogram or autocorrelation function as additional information. In SGS, each unsimulated grid node is visited sequentially in random order. Multi-Gaussian kriging is used to estimate a local cumulative distribution function (cdf) at each unknown grid node, conditioning to all the known and previously simulated data points, and the local cdf is randomly sampled to assign a

Table 2
Fluid properties [17,47]

	Water	PCE
ρ	0.9991	1.623 g/cm^3
μ	1.1139	0.89 cP
C_{eq}	N/A	203 mg/l
D_{m}	N/A	6.56×10^{-6} cm^2/s

Table 3
Variogram parameters for SGS geostatistical modeling [47]

Orientation	Nugget[a]	Variance[a,b]	Range (m)	Correlation length (m)
Horizontal	0.333	0.80	7.00	2.33
Vertical	0.333	1.00	1.07	0.36

[a] Variance normalized to 1.0.
[b] Includes nugget effect contribution.

simulated value at the node. This process continues until all unknown grid nodes have been determined. A full three-dimensional sequential Gaussian simulation was performed for each realization to incorporate site data. From each three-dimensional realization a vertical cross-section (7.92 m×9.75 m) was extracted and subsequently used for the simulation of a PCE infiltration event. This cross-section was oriented SW-NE along a flow path through the site's suspected DNAPL source zone. This extraction of a two-dimensional profile was done in the interest of computational tractability.

Simulated d_{10} values were used to calculate an intrinsic permeability field using a calibrated Carman–Kozeny equation. Available data from 167 repacked core samples from the site supported the assumption of a spatially uniform porosity of 0.360. Corresponding capillary properties in the cross-section were estimated using an average of measured air–water capillary pressure–saturation data and Leverett [49] scaling.

For the present study, three permeability realizations were chosen from the reference set of permeability realizations utilized by Lemke et al. [47]. These realizations were selected to encompass the variability of infiltration and entrapment behavior observed among the much larger ensemble of results simulated in that work. The second mass moment about the horizontal axis through the entrapped organic liquid's center of mass (i.e., vertical spreading) was selected as a representative DNAPL entrapment measure to distinguish among realizations:

$$\sigma_{M_x}^2 = \frac{\sum_i^{NN} (z_i - \bar{z})^2 S_{o_i} \phi_i \rho_{o_i} V_i}{\sum_i^{NN} S_{o_i} \phi_i \rho_{o_i} V_i} \tag{11}$$

where z_i is the is the z-coordinate of the ith node/element [L], NN is the number of nodes/elements in the domain, and V_i is the volume associated with the ith node/element [L^3]. $\bar{z}$ is the z-coordinate of the organic liquid's center of mass; the first spatial moment of the organic liquid distribution:

$$\bar{z} = \frac{\sum_i^{NN} z_i S_{o_i} \phi_i \rho_{o_i} V_i}{\sum_i^{NN} S_{o_i} \phi_i \rho_{o_i} V_i} \tag{12}$$

One permeability realization was selected to represent the mean behavior observed for the entire ensemble of entrapment results, and two realizations to represent spreading behavior that bounded the entire ensemble of
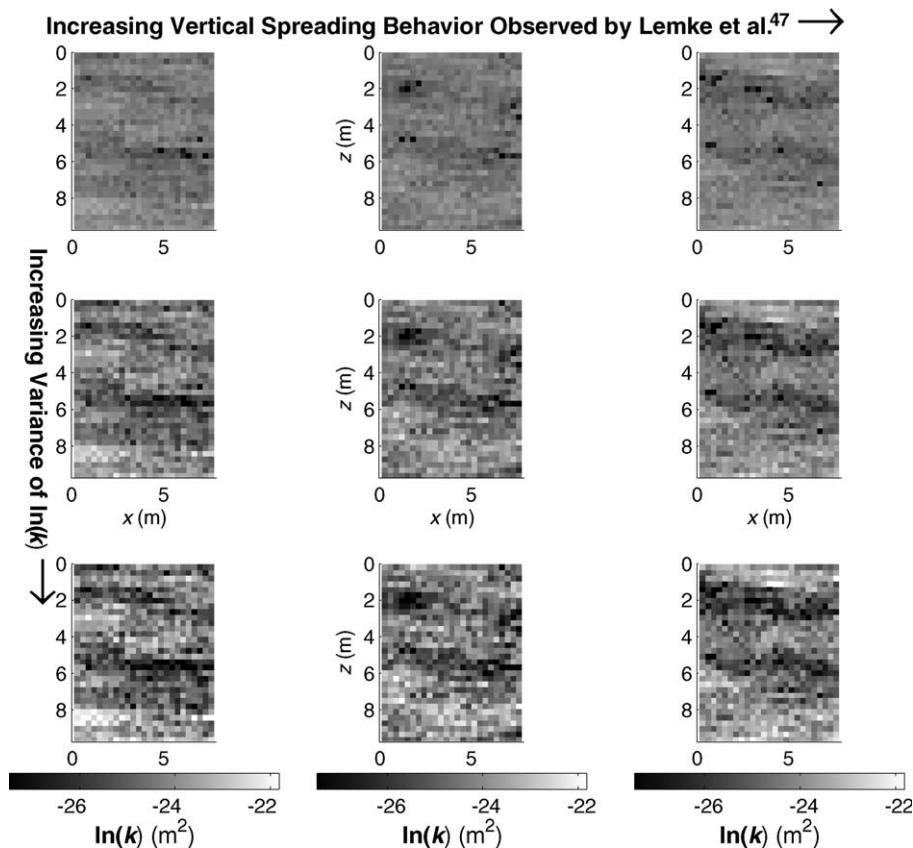

Fig. 1. Representative permeability realizations based upon work of Lemke et al. [47]. Increased vertical spreading is reproduced on the figure's horizontal axis (R1 → R2 → R3); increased ln(k) variance is reproduced on the figure's vertical axis (0.246 → 1.00 → 2.00).

entrapment results (a minimum and a maximum). These three reference cases will be referred to as cases R1 (minimum vertical spreading case, $\sigma^2_{M_x} = 2.19$ m^2), R2 (mean vertical spreading case, $\sigma^2_{M_x} = 4.41$ m^2), and R3 (maximum vertical spreading, $\sigma^2_{M_x} = 7.86$ m^2).

To examine the effect of different levels of heterogeneity, these three permeability realizations were then scaled to obtain six more distributions with identical $\ln(k)$ means but with larger $\ln(k)$ variances (1.00 and 2.00). [3] These additional values were chosen to reflect the range of $\ln(k)$ values observed in the literature (e.g., [41,68]) Data sets with $\ln(k)$ variances much higher than 2.50 are very rare. The nine permeability realizations are shown in Fig. 1.

There are relatively few data available that address the variability of wetting properties in the subsurface. Several studies, however, have explored the link between the spatial distribution of permeability and equilibrium sorption parameters. For example, the sorption capacity of the Borden aquifer material has been reported to be directly correlated with particle size [7]. Situations where sorption parameters might be inversely correlated with soil texture are also conceivable particularly in media where fines are higher in organic carbon. Thus, it is very difficult to make general statements about the relationship between permeability and sorption parameters. Several studies (e.g. [10,11,23,27,76]) have used an exponential relationship to positively or negatively correlate equilibrium sorption parameters to material permeability. Recognizing that the physicochemical basis behind many types of organic compound sorption also creates porous media surfaces which are strongly organic-wetting, this same type of correlation will be hypothesized for this study:

$$F_o = \widehat{F_o}e^{\Gamma[\ln(k)-\ln(\hat{k})]}, \quad 0 \leqslant F_o \leqslant 1 \tag{13}$$

Here, F_o is the mass fraction of organic-wet sand, $\widehat{F_o}$ is the geometric mean organic-wet mass fraction and Γ is the correlation coefficient. Four different wettability treatments were applied to the nine permeability fields to yield a completely water-wet ($F_o = 0.00$), completely organic-wet ($F_o = 1.00$), positively correlated ($\Gamma = +1.00$), and negatively correlated ($\Gamma = -1.00$) version

---

[3] Scaling was performed to preserve the mean but alter the variance of the permeability distributions

$$\ln(k)'_i = \sqrt{\frac{\sigma^2_{\ln(k)'}}{\sigma^2_{\ln(k)}}}(\ln(k)_i - \overline{\ln(k)}) + \overline{\ln(k)}$$

where $\ln(k)'_i$ is the scaled permeability value, $\sigma^2_{\ln(k)'}$ is the desired variance of the scaled permeability distribution, $\overline{\ln(k)}$ and $\sigma^2_{\ln(k)}$ are the mean and the variance of the original permeability distributions, and $\ln(k)_i$ is the original permeability value.

Table 4
Wettability parameters

Case	$\widehat{F_o}$	Γ
Water-wet	0.00	0.0
Organic-wet	1.00	0.0
Positively correlated	0.368[a]	+1.0
Negatively correlated	0.368[a]	−1.0

[a] 0.368 is approximately the geometric mean of F_o values ranging from 0 to 1.

$$\widehat{F_o} = e^{\frac{\int_0^1 \ln(F_o)dF_o}{1-0}} = e^{-1} \approx 0.368.$$

of each permeability field. These particular values of Γ were chosen to bracket the possible behavior observed when wettability is correlated to intrinsic permeability. When $\Gamma = -1.00$, organic-wet surfaces are associated with low-permeability zones and when $\Gamma = +1.00$, organic-wet surfaces are associated with high-permeability zones. Parameters used in (13) are summarized in Table 4. Fig. 2 shows a set of representative F_o values for a high variance $\ln(k)$ case in which $\Gamma = +1.00$. Aquifer properties are summarized in Table 5.

In aquifer settings, the time scale of interphase mass transfer is generally much larger than that of organic liquid infiltration. To reduce computational effort and decrease simulation run times, the infiltration and dissolution processes are decoupled in this investigation. Residual saturation distributions generated by M-VALOR were used as initial conditions for MISER simulations.

For the infiltration and entrapment simulations, the computational domain was discretized uniformly with 26 nodes horizontally ($\Delta x \sim 0.305$ m) and 128 nodes ($\Delta z = 0.0762$ m) vertically. Following the approach of Rathfelder and Abriola [60], Lemke et al. [47] performed an analysis of the sensitivity of spreading and maximum saturation behavior to vertical and horizontal grid refinement. The horizontal and vertical discretization used for this study is consistent with results of Lemke et al.'s analysis. No flow boundary conditions were imposed at the top and bottom of the domain while constant hydrostatic pressure boundary conditions were imposed on the left and right boundaries. Pertinent capillary model parameters are presented in Table 6.

The 36 (3 $\ln(k)$ variances × 4 wettability treatments × 3 realizations) final saturation distributions were then used as initial conditions for the simulations of mass removal using MISER. It was assumed that all organic liquid was immobile and that the only mechanism by which it could exit the domain was through aqueous phase transport. For the aqueous phase flushing simulations, a domain with the same spatial discretization was constructed for use in MISER. No-flow boundary conditions were employed at the top and bottom of the domain and a constant pressure boundary condition was specified on the left and right boundary such that a
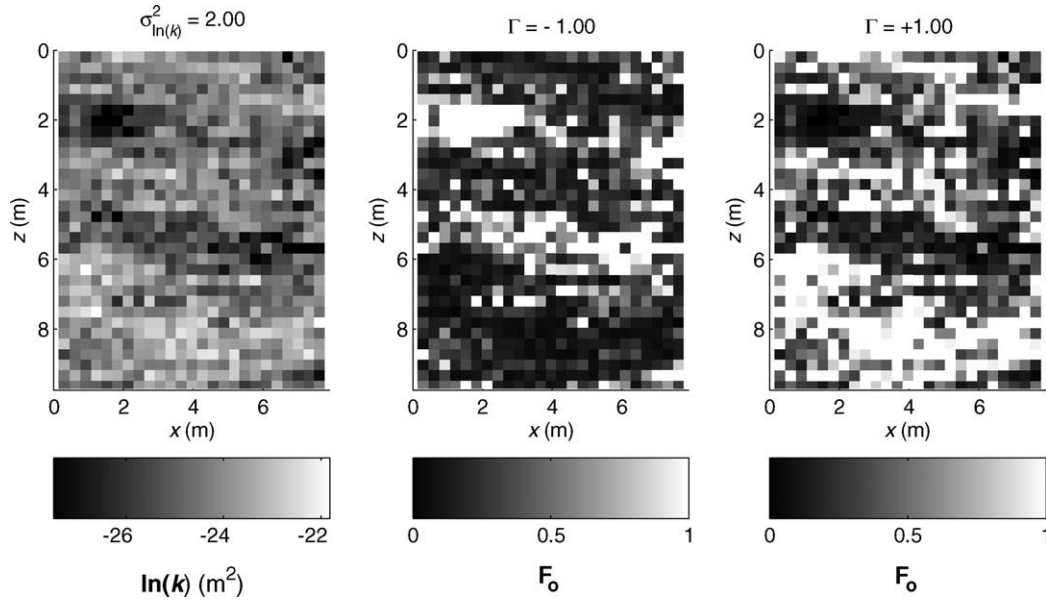
Fig. 2. Representative fractional wettability (F_o) distribution, obtained by correlation to permeability distribution.

Table 5
Soil properties [47]

	Low variance	Intermediate variance	High variance
ϕ	0.36	0.36	0.36
$\bar{k}_h (= k_{ref})$	1.971×10^{-11}	1.971×10^{-11}	1.971×10^{-11} m^2
$\sigma^2_{\ln(k)}$	0.246	1.00	2.00
$k_v : k_h$	1/2	1/2	1/2
U_i	1.86	1.86	1.86

Table 6
Capillary properties [47]

P_d	1860 Pa
λ	2.0773
S_{ra}	0.080
S_{ro}	0.151

piezometric head gradient of −0.130 (flow from left to right) was created. This value, while large, is consistent with forced flow conditions during a pilot-scale surfactant-enhanced aquifer remediation project conducted at the Oscoda dry cleaner site [28]. Imposed aqueous-phase component boundary conditions included no flux of organic solute at the top and bottom of the domain, zero total mass flux at the left side of the domain, and zero dispersive flux at the right side of the domain.

Utilization of the interphase mass transfer correlation presented in (10) requires knowledge of the spatial distribution of d_{50} values. Analysis of the original core data shows a linear relationship between d_{50} and d_{10} values (cf. Fig. 3). A simple linear regression relationship was used to estimate a spatial d_{50} field from the spatial d_{10} field generated by the sequential Gaussian simulations.

$$d_{50} = 1.24 d_{10} + 61.9 \ \mu m$$
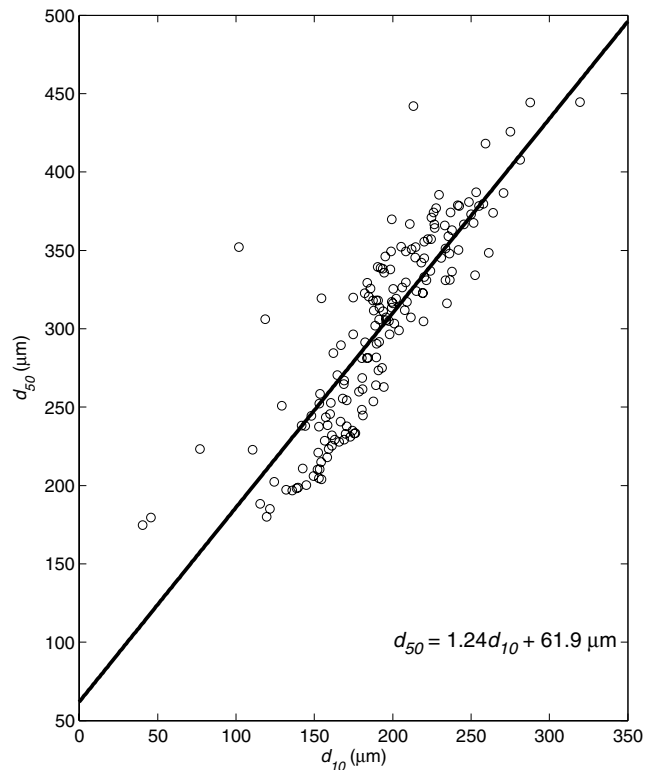
Fig. 3. Relationship between d_{50} and d_{10} for Bachman soil samples.

4. Results

Fig. 4 presents organic liquid distributions for the mean spreading behavior simulations (R2). These results are representative of the behavior observed in the larger suite of 36 infiltration simulations. Some overall trends
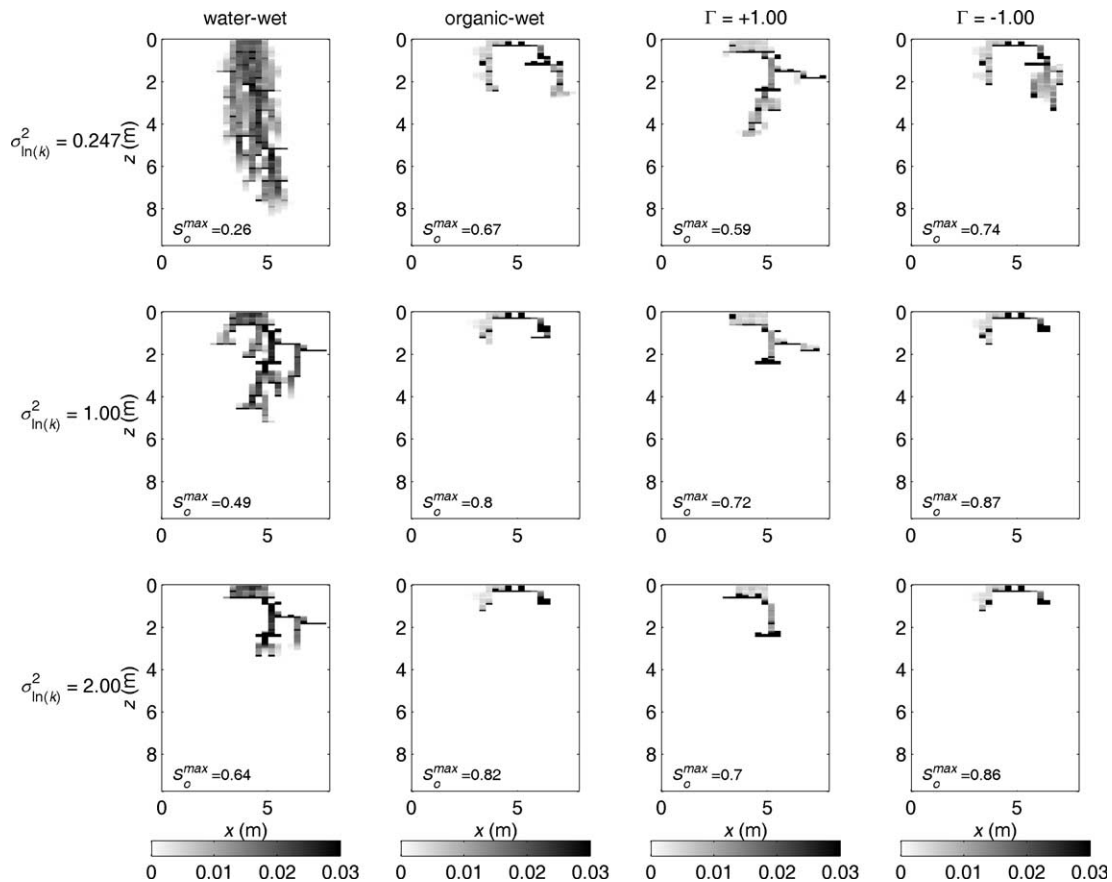
Fig. 4. Representative residual organic distributions. Here, the mean spreading behavior results are presented (R2).

are directly observable from Fig. 4. Incorporation of organic-wet surfaces tends to increase the magnitude of maximum DNAPL saturations. The depth of penetration and extent of vertical spreading is reduced as $\sigma^2_{\ln(k)}$ increases. This result is consistent with previous studies. [24,31,43,47].

A spatial moment analysis was performed to quantitatively investigate entrapment behavior. Three metrics were selected to quantify the spatial distribution of DNAPL in the simulated systems. Depth of penetration was represented by the z-coordinate of the organic liquid's center of mass, the first spatial moment of the organic liquid distribution (12). The degree of horizontal and vertical spreading was quantified via the square root of the second spatial moment of the organic liquid distribution, the radii of gyration $((\sigma^2_{M_z})^{1/2}$ and $(\sigma^2_{M_x})^{1/2}$, cf. Eq. (11)) about the z-axis and x-axis (respectively) passing through the organic liquid's center of mass. In addition, the maximum organic liquid saturation encountered in the domain was determined. Similar metrics have been used in several previous investigations. [24,31,43,47].

Fig. 5 presents maximum organic liquid saturation for each of the permeability and organic-wet mass fraction distributions. Mean behavior among the three realizations for each permeability field (R1–R3) along

with 95% confidence intervals are presented. Consistent with earlier studies [13,24], inspection of Fig. 5 suggests that the magnitude of maximum organic liquid saturation increases with increasing values of $\sigma^2_{\ln(k)}$. Organic liquids tend to pool at interfaces of capillary property contrast which are more prevalent in systems with higher $\ln(k)$ variances. Fig. 5 also suggests that the inclusion of organic-wet materials increases the magnitude of maximum organic liquid saturations. It appears that there is no significant difference between the positively correlated, negatively correlated, and completely organic-wet systems. This would suggest that the presence of organic-wet media, regardless of its correlation to permeability, tends to generate high organic liquid saturations.

Fig. 6 presents a summary of depth of penetration results for each of the twelve permeability and fractional wettability combinations. The behavior observed here is similar to that of maximum saturation. Organic liquid tends to penetrate less in systems with higher variability in $\ln(k)$, owing to the increased incidence of capillary property contrasts. Similarly, inclusion of organic-wet solids tends to reduce depth of penetration with little difference seen among the positively correlated, negatively correlated, and completely organic-wet systems. In systems with at least some portion of organic-wet
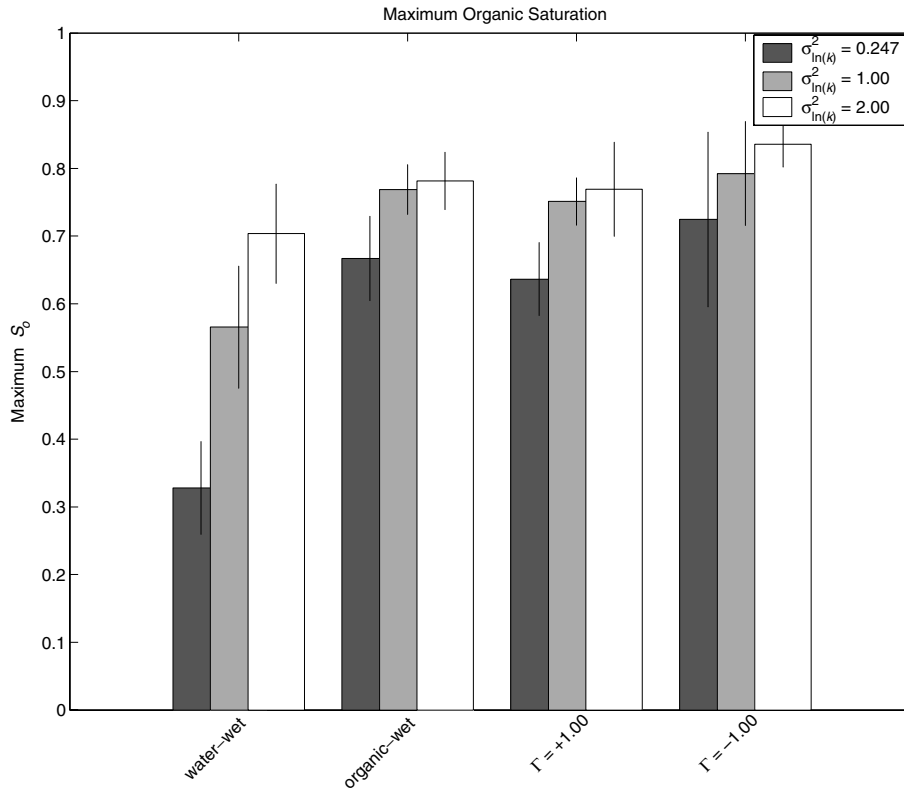
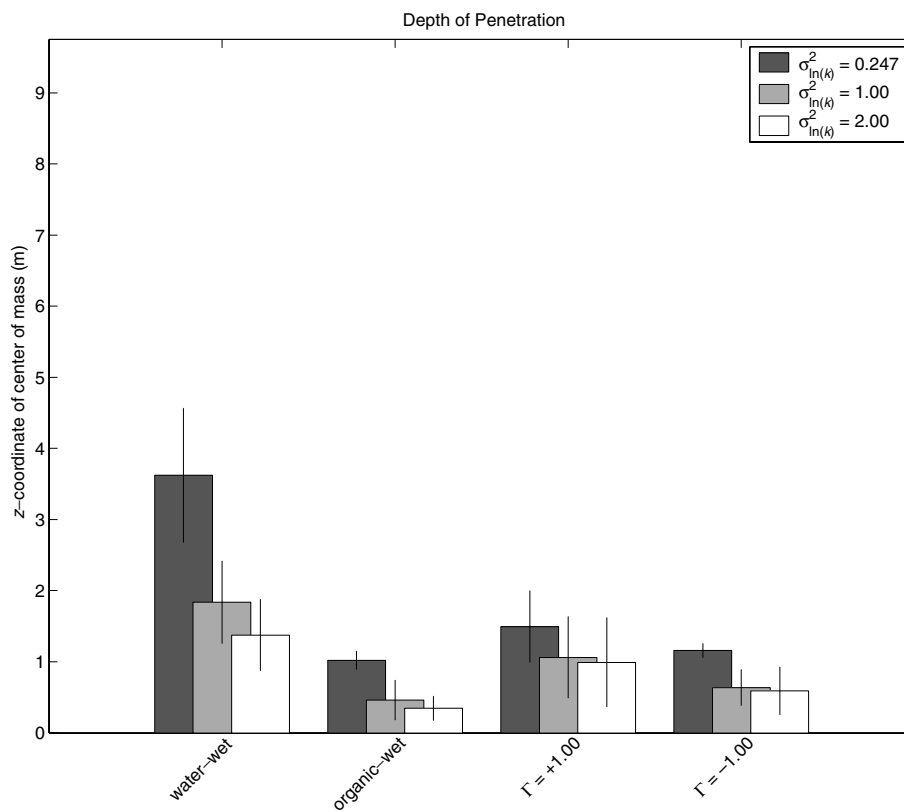Fig. 5. Maximum organic saturation as a function of $\ln(k)$ variance and fractional wettability.

Fig. 6. Depth of organic penetration as a function of $\ln(k)$ variance and fractional wettability.

solids present, the organic liquid resides in areas that are more strongly organic-wetting. In order for the organic liquid to penetrate into a deeper layer that is perhaps less organic-wetting, high saturations are needed to overcome the positive entry pressure of the lower layer. Fig. 7 presents vertical spreading metrics for the twelve systems. Analogous behavior is observed. Vertical spreading is reduced in systems with higher $\ln(k)$ variances and systems where some portion of organic-wet solids are present.

Fig. 8 presents horizontal spreading metrics for these simulations. Here, the radius of gyration, σ_{M_z}, is plotted relative to the horizontal radius of gyration of the spill zone ($= w^2/12$, where w is the width of the spill area). In other words, the radius of gyration is normalized to the value that an organic liquid distribution would have had it infiltrated uniformly from the spill zone without any horizontal spreading. There does not appear to be any discernable trend in horizontal spreading with $\ln(k)$ variance or organic-wetting characteristics. Kueper and Gerhard [44] found that horizontal spreading metrics often do not converge to an ensemble average. In addition, the variability of horizontal spreading metrics decreases with increasing spill width relative to the horizontal correlation length [24]. In the present study, the spill width is slightly more than one half the correlation length (1.22 m vs. 2.33 m).

The three permeability realizations taken from Lemke et al. [47] (R1–R3, $\sigma^2_{\ln(k)} = 0.246$) were chosen to reflect the variability of vertical spreading behavior observed in that study. It was anticipated that the relative magnitude of vertical spreading metrics (i.e., $^{R1}\sigma^2_{M_x} < {}^{R2}\sigma^2_{M_x} < {}^{R3}\sigma^2_{M_x}$) would be preserved when the permeability distributions were scaled to obtain $\ln(k)$ variances of 1.00 and 2.00. It was reasoned that although the scaling process might change the relative magnitude of $\ln(k)$ values, it would not alter the overall architecture of the aquifer thereby preserving flow pathways. Spatial moment analyses revealed that this was not the case at the high $\ln(k)$ variance (2.00). In these simulations, the realization that gave the maximum vertical spreading in the water-wet $\sigma^2_{\ln(k)} = 0.246$ and $\sigma^2_{\ln(k)} = 1.00$ systems (R3) actually gave the minimum vertical spreading behavior when $\sigma^2_{\ln(k)} = 2.00$. For this $\ln(k)$ variance, the relative order of vertical spreading magnitudes was $^{R3}\sigma^2_{M_x} < {}^{R1}\sigma^2_{M_x} < {}^{R2}\sigma^2_{M_x}$.

Analyses of simulation results do not reveal a significant difference in maximum organic liquid saturation, depth of penetration, or vertical spreading values among the three $\ln(k)$ variances for the organic-wet, positively correlated, and negatively correlated systems. When compared to the clear dependence on $\ln(k)$ variance demonstrated by the water-wet sands, this suggests that the presence of organic-wet solids may potentially
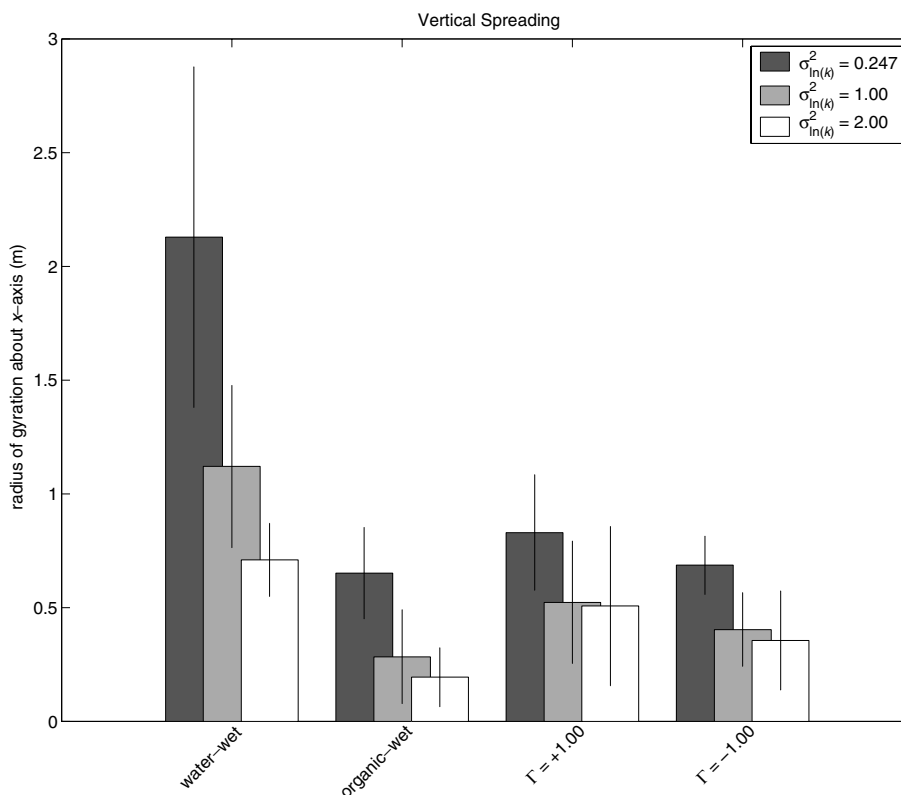

Fig. 7. Degree of vertical spreading as a function of $\ln(k)$ variance and fractional wettability.
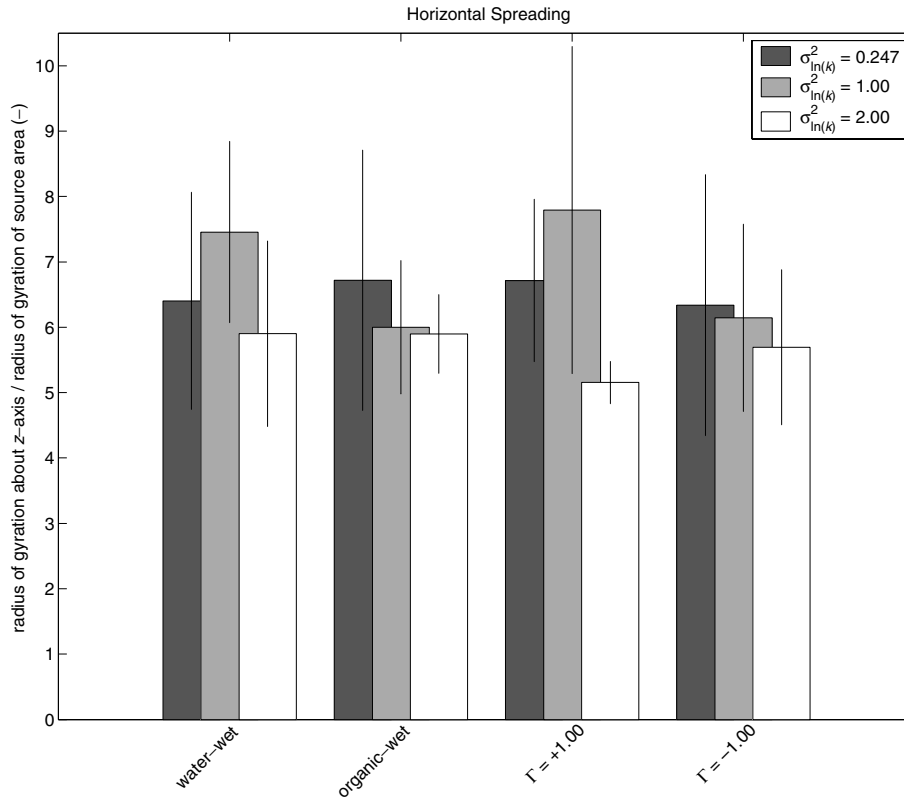
Fig. 8. Degree of horizontal spreading as a function of $\ln(k)$ variance and fractional wettability.

reduce the impact of $\ln(k)$ variance on DNAPL migration and entrapment.

It may be hypothesized that the permeability and organic-wet mass fraction characteristics of the zones in which the organic liquid resides will exert a controlling influence over the rates and extent of interphase mass transfer and DNAPL mass removal. Clearly permeability will control accessibility and, since aqueous phase velocity (a linear function of permeability) and organic-wet mass fraction are the spatially variable parameters incorporated into the Sherwood number mass transfer correlation, these parameters will also control the local interphase mass transfer rate (see Eq. (10)).

Fig. 9 presents a mass histogram for two of the water-wet and organic-wet systems ($\sigma^2_{\ln(k)} = 1.00$, R1 and $\sigma^2_{\ln(k)} = 2.00$, R3). Here, the distribution of the entrapped organic liquid mass is depicted as a function of the medium permeability with which it is associated. In one case ($\sigma^2_{\ln(k)} = 2.00$), the organic liquid is distributed over a wide range of $\ln(k)$ values for both the completely water-wet and completely organic-wet systems. In the other ($\sigma^2_{\ln(k)} = 1.00$), the majority of the organic liquid is located in higher permeability zones in the water-wet systems and in the lower permeability zones in the organic-wet systems. Fig. 10 presents percent mass removed over time (pore volumes) during the flushing simulations and the evolution of the Darcy-flux averaged concentration on the downstream boundary for

these four scenarios. Here it can be seen that in systems where the organic liquid is distributed uniformly across permeabilities there is little difference in the rate that organic liquid is removed from the system or in the flux-averaged concentrations at the downstream boundary. In contrast, systems where the organic liquid is located in higher permeability zones exhibit higher initial rates of mass removal and correspondingly higher flux-averaged concentration values, caused by both the high interphase mass transfer rate (due to a higher Reynolds number) and greater accessibility of the aqueous phase to entrapped organic liquid. Concentrations in these water-wet systems drop off rapidly and do not exhibit the pronounced tailing behavior found in the organic-wet systems. This tailing behavior is hypothesized to be due to the slow dissolution of organic liquid from low-permeability zones. Although sorption processes have been neglected here, they would be expected to play a larger role in increasingly organic-wet systems [17] which would contribute further to the tailing behavior observed in the organic-wet systems.

Results indicate that mass removal efficiency in these systems appears to be highly realization dependent. Thus, it may not be possible to correlate the permeability of the material containing DNAPL with its particular wettability characteristics, i.e., the organic liquid may not always exist in the low permeability zones of an organic-wet material or in the high permeability zones of
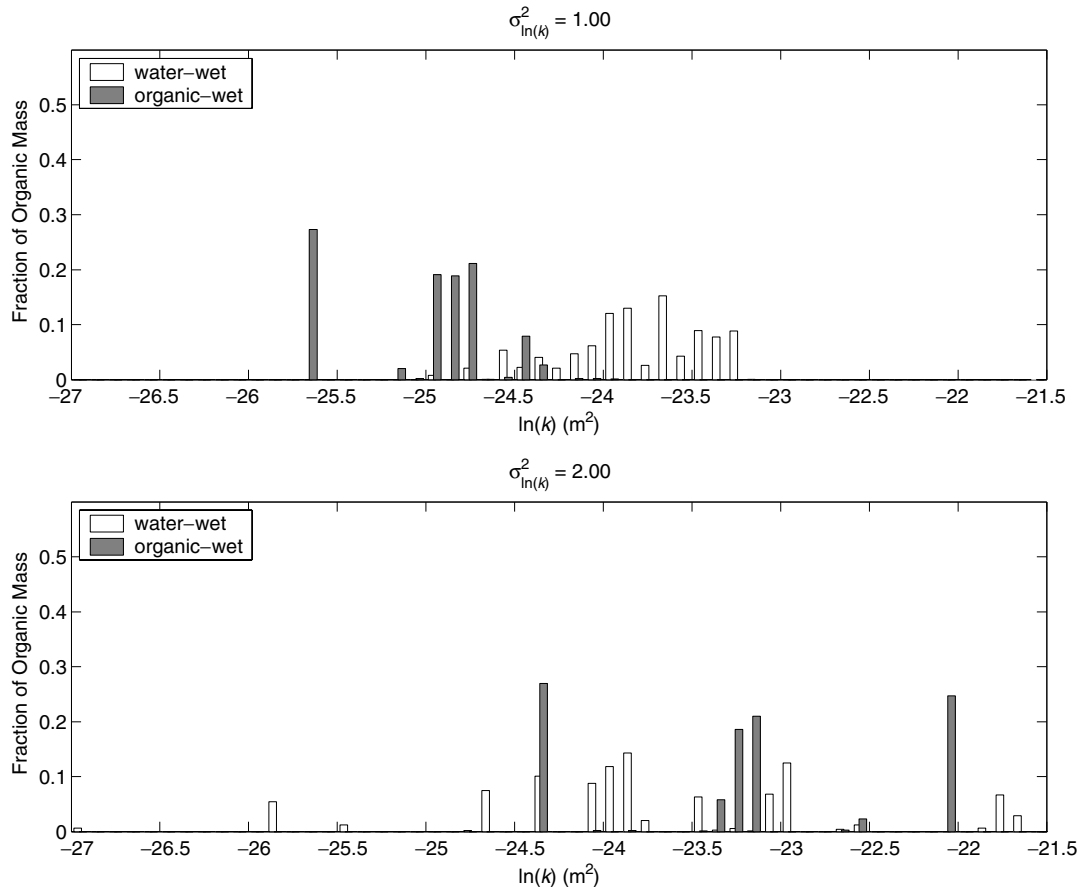
Fig. 9. Spatial co-location of aquifer parameters and organic mass in completely water and organic-wet systems.

a water-wet material. Fig. 11 is a composite plot of the organic liquid mass residence histograms for the geostatistical realizations depicted in Fig. 1. Here the histograms for the completely water-wet and completely organic-wet systems are presented. For each of the three $\ln(k)$ variances employed (shown on the vertical axis), there is no consistent behavior among the three realizations that were examined (shown on the horizontal axis). For example, consider the $\sigma^2_{\ln(k)} = 2.00$ case (bottom row of Fig. 11). In two of the realizations (R1 and R3, on the left and right sides of the bottom row) the DNAPL exists within a broad range of the permeability values for both completely organic-wet and water-wet systems. Contrast this behavior with the R2 realization (center plot), where the DNAPL exists in low permeability zones in the organic-wet system and in high permeability zones in the water-wet system. Similar conclusions may be drawn about the lower $\ln(k)$ variance results shown in Fig. 11. As mass recovery appears to be governed by the permeability of the DNAPL containing zones, it may not be possible to draw conclusions about organic liquid mass recovery based solely upon aquifer geostatistics and wettability characteristics.

Several additional simulations were performed to assess the sensitivity of model predictions to the inter-

phase mass transfer rates. The lumped liquid film mass transfer coefficient, $\hat{k}^{ao}_l$, was varied over an order of magnitude. Model predictions (not presented here) demonstrated little sensitivity of the aqueous phase concentration or mass removal rates to the mass transfer coefficient. This suggests that wettability does not exert a controlling influence through the mass transfer coefficient. It does, however, influence the distribution of DNAPL and, consequently, mass recovery.

There has been debate in the literature regarding the usefulness of source zone mass removal as a means of remediating contaminated aquifers [58,67]. Fig. 12 presents a composite plot of effluent concentration reduction vs. mass removal for the simulations presented in Fig. 11. Effluent concentration reduction is presented relative to the maximum effluent concentration observed on the downstream boundary (χ_{max}), which is noted on each plot. Simulations that do not reach 100% on both axes were not of long enough duration to realize full contaminant removal. Results show that water-wet systems exhibit higher maximum effluent concentration values than the corresponding organic-wet systems. This behavior can be attributed to the rapid initial dissolution of organic liquid entrapped in the high permeability zones of a water-wet system. In addition, with the
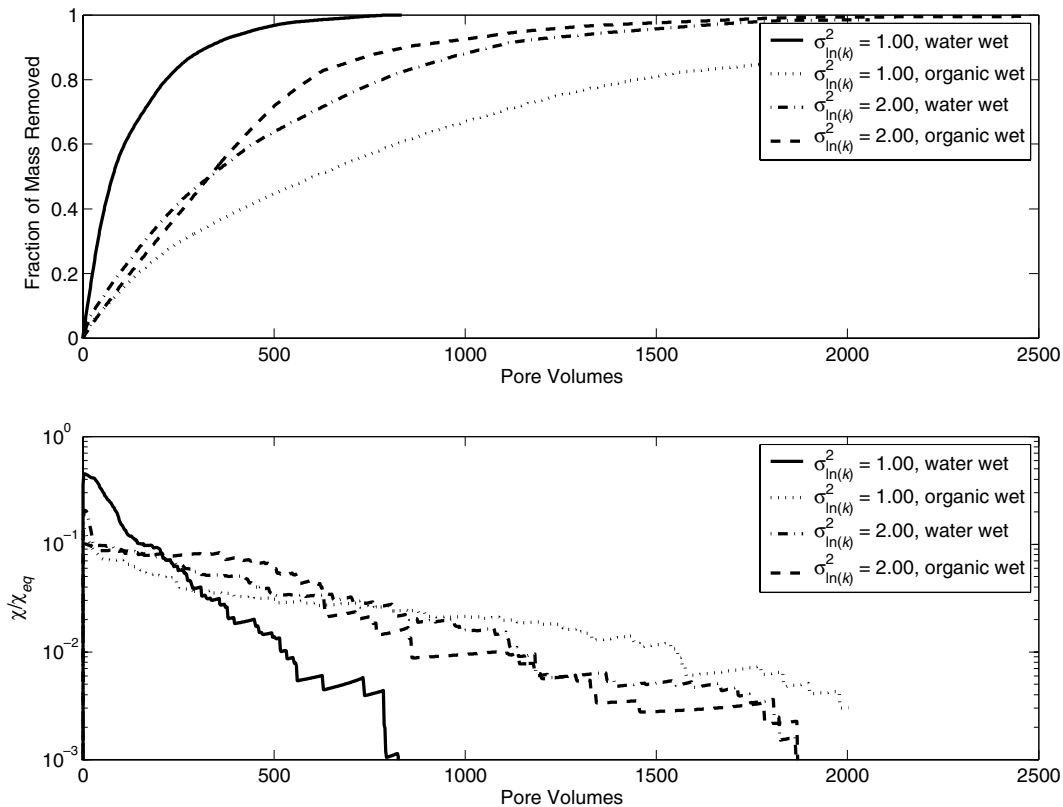
Fig. 10. Mass recovery behavior for systems depicted in Fig. 9.

exception of the one simulation (organic-wet, $\sigma^2_{\ln(k)} = 1.00$, R3) maximum effluent concentrations appear to decrease with increasing $\ln(k)$ variance.

Fig. 12 also demonstrates that significant differences in mass removal behavior are found among members of this suite of simulations. There does not appear to be a trend in mass removal with respect to $\ln(k)$ variance or wettability characteristics. In the three $\sigma^2_{\ln(k)} = 0.246$ realizations, the organic-wet systems exhibit rapid effluent concentration reduction with modest amounts of mass removal, but then show decreased rates of effluent concentration reduction with additional mass removal. Conversely, the water-wet systems exhibit slow concentration reduction initially, followed by a rapid decrease as the last portion of organic liquid mass is removed. Realizations R1 and R3 of the $\sigma^2_{\ln(k)} = 2.00$ simulations, however, exhibit the opposite behavior and realization R1 of the $\sigma^2_{\ln(k)} = 1.00$ simulations reveals very similar behavior for both the organic- and water-wet systems.

Fig. 12 suggests that it is possible to correlate aqueous phase concentrations to source zone architecture, but it may not be possible to correlate mass removal performance (concentration reduction as a function of mass removal) to permeability and wettability characteristics of the organic liquid bearing materials. For example, realization R1 of the $\sigma^2_{\ln(k)} = 1.00$ simulations shows that the organic liquid is distributed in very dif-

ferent permeability media (cf. Fig. 11) and this is reflected in the magnitude of the effluent concentrations. The mass removal behavior of these systems (cf. Fig. 12), however, are remarkably similar.

The observation that mass removal behavior is not correlated to aquifer geostatistics and wettability characteristics may be a function of the Gaussian model used to generate the permeability fields used in this investigation. A recognized limitation of sequential Gaussian simulation is its inability to preserve the occurrence of continuous stratigraphic units because of its tendency to maximize the entropy associated with a given realization [34,35,40]. Further investigations are necessary to determine if alternative geostatistical conceptualizations of subsurface variability demonstrate different mass removal behavior.

5. Conclusions

A comprehensive mathematical model is presented that incorporates the effects of fractional wettability on organic liquid infiltration, retention, and dissolution in the saturated zone. The model is based on previous investigations that examined the effect of fractional wettability on these processes individually.

Geostatistical realizations of spatial distributions of intrinsic permeability were generated using sequential
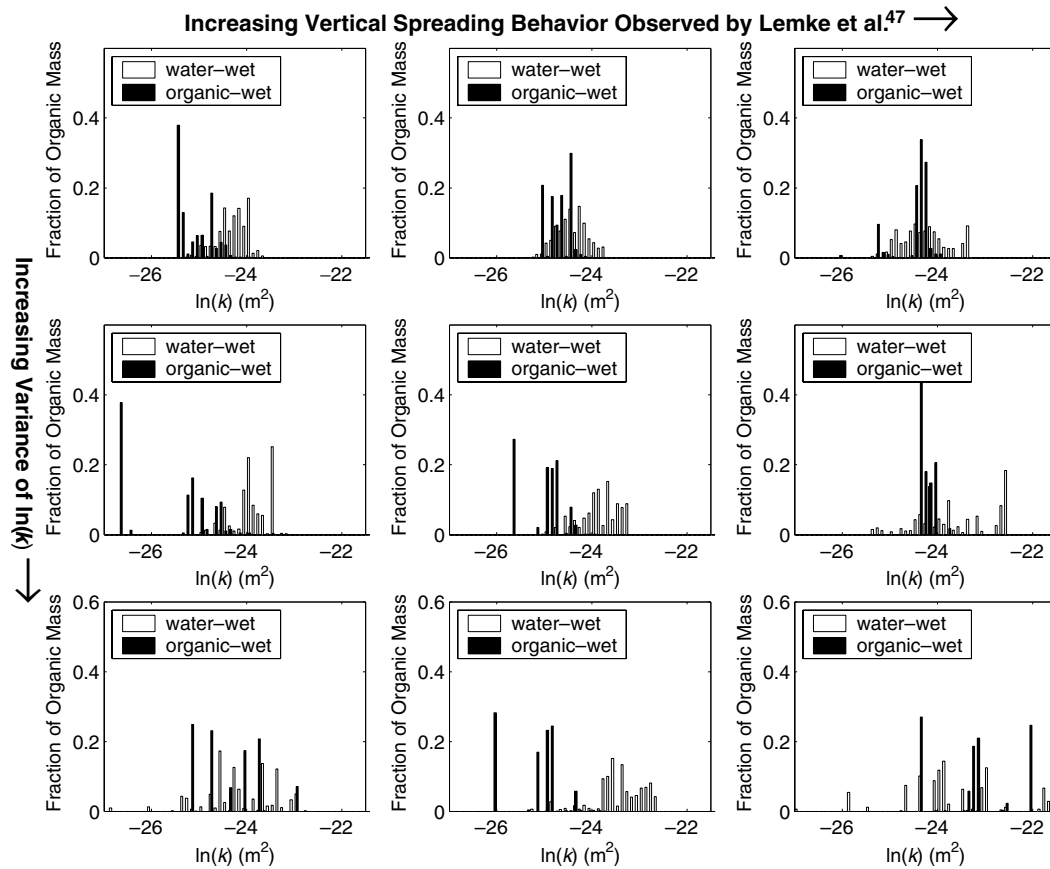
Fig. 11. Spatial co-location of aquifer parameters and organic mass for water-wet and organic-wet treatments of geostatistical realizations presented in Fig. 1. Increased vertical spreading is reproduced on the figure's horizontal axis (R1→R2→R3); increased ln(k) variance is reproduced on the figure's vertical axis (0.246 →1.00→2.00).

Gaussian simulation conditioned to data collected from a surficial glacial aquifer in the Lower Peninsula of Michigan. Chemical heterogeneity, in the form of fractional wettability, was correlated to physical heterogeneity through an exponential correlation. Organic liquid saturation distributions were developed using a modified form of the finite-difference multiphase flow code M-VALOR. A spatial moment analysis was performed on these results to discern the potential effect of coupled physical and chemical heterogeneity on predictions of organic liquid migration and entrapment. These results were also used in a compositional flow and transport simulator to examine the effect of fractional wettability on predictions of organic liquid mass dissolution and recovery.

Results suggest that fractional wettability can have a significant impact on the migration and entrapment of PCE in aquifers. The occurrence of organic-wet solids in heterogeneous systems tends to reduce depths of penetration, increase the magnitude of entrapped organic liquid saturations, and decrease the extent of vertical spreading. This behavior is consistent with an organic liquid's preferential tendency to reside in systems that are thermodynamically favorable, i.e., organic-wet sys-

tems. The presence of organic-wet solids also appears to reduce the impact of ln(k) variance.

Spatial moment analysis results indicated that horizontal spreading was not affected by this coupled physical and chemical heterogeneity, although this is in disagreement with previous studies. It is hypothesized that this conclusion is attributed to the size of the release area with respect to the horizontal correlation length.

Simulations of mass recovery revealed that the permeability and wettability of the zones containing the organic liquid mass exert a controlling effect on mass recovery efficiency and aqueous phase effluent concentrations. In systems where organic liquids are entrapped in higher permeability zones, mass transfer is higher yielding fast mass recovery, higher initial aqueous phase effluent concentrations, and limited concentration tailing behavior. The opposite behavior is seen in systems where organic liquids are entrapped in lower permeability zones. In heterogeneous systems, wettability does not exert a controlling influence through variations in the mass transfer coefficient but rather through controls on infiltration behavior.

Results suggest that subsurface distributions of organic liquids in aquifers with correlated permeability
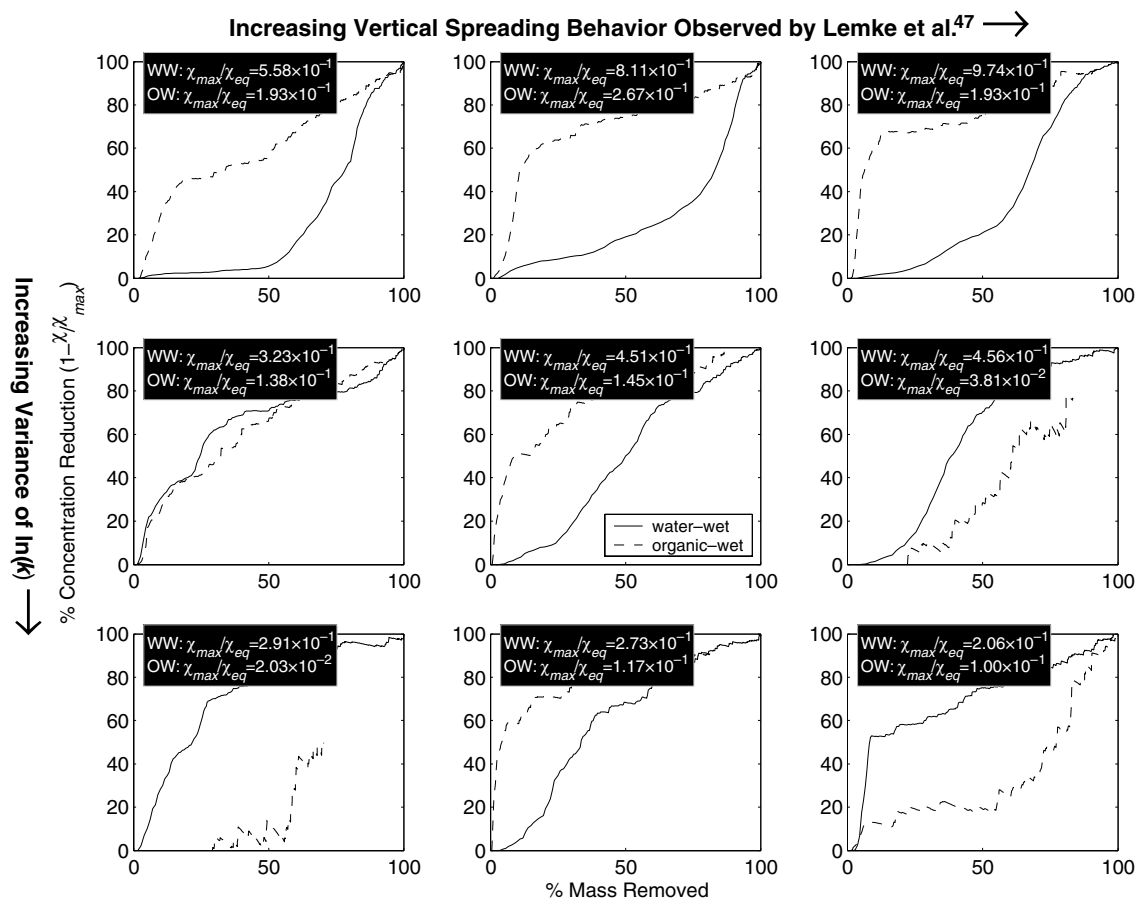
Fig. 12. Percent concentration reduction as a function of mass removal for the simulations presented in Fig. 11. Increased vertical spreading is reproduced on the figure's horizontal axis (R1 → R2 → R3); increased $\ln(k)$ variance is reproduced on the figure's vertical axis ($0.246 \to 1.00 \to 2.00$). Concentration reduction is defined as the effluent concentration value (χ) normalized to the maximum effluent concentration observed over the entire simulation (χ_{max}). Also noted are the maximum effluent concentration values observed normalized to the equilibrium solubility of PCE in water (χ_{max}/χ_{eq}).

and wettability characteristics may be highly realization dependent. Thus it is difficult to draw conclusions about organic liquid mass removal efficiency based solely on geostatistical and wettability characteristics. Further work is necessary to explore the effects of alternative geostatistical conceptualizations of aquifer heterogeneity and alternative permeability/wettability correlations on predictions of DNAPL infiltration and mass recovery.

References

[1] Abriola LM. Modeling multiphase migration of organic chemicals in groundwater systems—a review and assessment. Environ Health Perspect 1989;83:117–43.

[2] Abriola LM, Lang J, Rathfelder K. Michigan soil vapor extraction remediation (MISER) model: a computer program to model soil vapor extraction and bioventing of organic chemicals in unsaturated geological material, United States Environmental Protection Agency, 1997.

[3] Abriola LM, Rathfelder KM, Maiza M, Yadav S. VALOR code version 1.0: a PC code for simulating immiscible contaminant transport in subsurface systems, EPRI TR-101018, Project 2879-08, Final Report, 1992.

[4] Anderson WG. Wettability literature survey—Part 1: Rock/oil/brine interactions and the effects of core handling on wettability. J Petroleum Technol 1986;38:1125–44.

[5] Anderson WG. Wettability literature survey—Part 4: Effects of wettability on capillary pressure. J Petroleum Technol 1987;39:1283–300.

[6] Anderson WG. Wettability literature survey—Part 5: The effect of wettability on relative permeability. J Petroleum Technol 1987;39:1453–68.

[7] Ball WP, Roberts PV. Long-term sorption of halogenated organic chemicals by aquifer material. 1. Equilibrium. EST 1991;25:1223–36.

[8] Barth G, Illangasekare T, Rajaram H, Ruan H. Model calibration and verification for entrapped NAPL using tracer tests in a large, two-dimensional tank with heterogeneous packing. Wallingford, Engl.: Golden, CO, USA: IAHS Press; 1996.

[9] Bear J. Dynamics of fluids in porous media. New York, NY: Elsevier; 1972.

[10] Bellin A, Rinaldo A, Bosma WJP, Zee SEATMvd, Rubin Y. Linear equilibrium adsorbing solute transport in physically and chemically heterogeneous porous formations. 1. Analytical solutions. WRR 1993;29:4019–31.

[11] Bosma WJP, Bellin A, Zee SEATMvd, Rinaldo A. Linear equilibrium adsorbing solute transport in physically and chemically heterogeneous porous formations, 2. Numerical results. WRR 1993;29:4031–43.

[12] Bradford SA, Abriola LM, Leij FJ. Wettability effects on two- and three-fluid relative permeabilities. JCH 1997;28:171–91.

[13] Bradford SA, Abriola LM, Rathfelder KM. Flow and entrapment of dense nonaqueous phase liquids in physically and chemically heterogeneous aquifer formations. AWR 1998;22:117–32.

[14] Bradford SA, Leij FJ. Fractional wettability effects on two- and three-fluid capillary pressure–saturation relations. JCH 1995;20:89–109.

[15] Bradford SA, Leij FJ. Wettability effects on scaling two- and three-fluid capillary pressure–saturation relations. EST 1995;29:1446–55.

[16] Bradford SA, Leij FJ. Predicting two- and three-fluid capillary pressure–saturation relationships of porous media with fractional wettability. WRR 1996;32:251–9.

[17] Bradford SA, Phelan TJ, Abriola LM. Dissolution of residual tetrachloroethylene in fractional wettability porous media: Correlation development and application. JCH 2000;45:35–61.

[18] Bradford SA, Rathfelder KM, Lang J, Abriola LM. Entrapment and dissolution of DNAPLs in heterogeneous porous media. JCH 2003;67:133–57.

[19] Bradford SA, Vendlinski RA, Abriola LM. The entrapment and long-term dissolution of tetrachloroethylene in fractional wettability porous media. WRR 1999;25:2955–64.

[20] Brooks RH, Corey AT. Properties of porous media affecting fluid flow. J Irr Dr Div Am Soc Civ Eng 1966;92:61–88.

[21] Brown CL, Pope GA, Abriola LM, Sepehrnoori K. Simulation of surfacant-enhanced aquifer remediation. WRR 1994;30:959–2977.

[22] Burdine NT. Relative permeability calculations from pore size distribution data. Petroleum Trans, AIME 1953;198:71–8.

[23] Cvetkovic VD, Shapiro AM. Mass arrival of sorptive solute in heterogeneous porous media. WRR 1990;26:2057–67.

[24] Dekker TJ, Abriola LM. The influence of field-scale heterogeneity on the infiltration and entrapment of dense nonaqueous phase liquids in saturated formations. JCH 2000;42:187–218.

[25] Dekker TJ, Abriola LM. The influence of field-scale heterogeneity on the surfactant-enhanced remediation of entrapped nonaqueous phase liquids. JCH 2000;42:219–51.

[26] Demond AH, Rathfelder K, Abriola LM. Simulation of organic liquid flow in porous media using estimated and measured transport properties. JCH 1996;22:223–39.

[27] Destouni G, Cvetkovic V. Field scale mass arrival of sorptive solute into the groundwater. WRR 1991;27:1315–25.

[28] Drummond CD, Lemke LD, Rathfelder KM, Hahn EJ, Abriola, LM. In: Wickramanayake GB, Gavaskar AR, Gupta N, editors. Treating dense nonaqueous phase liquids (DNAPLs): Remediation of chlorinated and recalcitant compounds. Columbus, OH: Batelle Press; 2000. p. 77–84.

[29] Dubey ST, Doe PH. Base number and wetting properties of crude oils. SPE Reservoir Eng 1993;9:195–200.

[30] Essaid HI, Herkelrath WN, Hess KM. Simulation of fluid distributions observed at a crude oil spill site incorporating hysteresis, oil entrapment, and spatial variability of hydraulic properties. WRR 1993;29:1753–70.

[31] Essaid HI, Hess KM. Monte Carlo simulations of multiphase flow incorporating spatial variablility of hydraulic properties. GW 1993;31:123–34.

[32] Fountain JC, Starr RC, Middleton T, Beikirch M, Taylor C, Hodge D. Controlled field test of surfactant-enhanced aquifer remediation. GW 1996;34:910–6.

[33] Gaudin AM, Decker TG. Contact angles and adsorption in the system quartz-water-dodecane modified by dodecyl ammonium chloride. J Coll Interf Sci 1967;24:151–8.

[34] Gómez-Hernández JJ. Issues on environmental risk assessment, vol. 1. Kluwer Academic Publishers; 1996.

[35] Gómez-Hernández JJ, Wen X-H. To be or not to be multi Gaussian? A reflection on stochastic hydrogeology. AWR 1998;21:47–61.

[36] Haley JL, Hanson B, Enfield C, Glass J. Evaluating the effectiveness of groundwater extraction systems. Ground Water Monitor Rev 1991;11:119–24.

[37] Illangasekare TH, Armbruster EJ, Yates DN. Non-aqueous-phase fluids in heterogeneous aquifers—experimental study. J Environ Eng 1995;121:571–9.

[38] Jennings HY. A sudy of caustic solution-crude oil interfacial tensions. Soc Petroleum Engr J 1975;15:197–202.

[39] Jerauld GR. General three-phase relative permeability model for Prudhoe Baym. UAE: Society of Petroleum Engineers: Abu Dhabi; 1996.

[40] Journel AG, Deutsch CV. Entropy and spatial disorder. Math Geol 1993;25:329–55.

[41] Jussel P, Stauffer F, Dracos T. Transport modeling in heterogeneous aquifers: 1. Statistical description and numerical generation of gravel deposits. WRR 1994;30:1803–17.

[42] Kovscek AR, Wong H, Radke CJ. A pore-level scenario for the development of mixed wettability in oil reservoirs. AIChE J 1993;39:1072–85.

[43] Kueper BH, Frind EO. Two-phase flow in heterogeneous porous media. 2. Model application. WRR 1991;27:1059–70.

[44] Kueper BH, Gerhard JI. Variability of point source infiltration rates for two-phase flow in heterogeneous porous media. WRR 1995;31:2971–80.

[45] Kueper BH, Redman D, Starr RC, Reitsma S, Mah M. A field experiment to study the behavior of tetrachloroethylene below the water table: spatial distribution of pooled DNAPL. GW 1993;31:756–66.

[46] Lemke LD, Abriola LM. Predicting DNAPL entrapment and recovery: the influence of hydraulic property correlation. Stoch Environ Res Risk Assess 2003;17:408–18.

[47] Lemke LD, Abriola LM, Goovaerts P. DNAPL source zone characterization: Influence of hydraulic property correlation on predictions of DNAPL infiltration and entrapment. WWR, in press.

[48] Lenhard RJ, Oostrom M. A parametric model for predicting relative permeability–saturation–capillary pressure relationships of oil–water systems in porous media with mixed wettability. TPM 1998;31:109–31.

[49] Leverett MC. Capillary behavior in porous solids. AIME Trans: Petroleum Develop Technol Div 1941;142:152–69.

[50] Lord DL. Influence of organic acid and base solution chemistry on interfacial and transport properties of mixed wastes in the subsurface. Ann Arbor, MI: University of Michigan; 1999.

[51] McDougall SR, Sorbie KS. The prediction of waterflood performance in mixed-wet systems from pore-scale modelling and simulation. New Orleans, LA: Society of Petroleum Engineers; 1993.

[52] Mercer JW, Skipp DC, Giffin, D. Basics of pump-and-treat ground-water remediation technology, EPA, R.S. Kerr Environmental Research Lab, 1990.

[53] Morrow NR. Effects of surface roughness on contact angle with special reference to petroleum recovery. J Can Petroleum Technol 1975;14:42–53.

[54] Mualem Y. A new model for predicting the hydraulic conductivity of unsaturated porous media. WRR 1976;12:513–22.

[55] Poulsen M, Kueper BH. A field experiment to study the behavior of tetrachloroethylene in unsaturated porous media. EST 1992;26:889–95.

[56] Powers SE, Anckner WH, Seacord TF. Wettability of NAPL-contaminated sands. J Environ Eng 1996;122:889–96.

[57] Powers SE, Tamblin ME. Wettability of porous media after exposure to synthetic gasolines. JCH 1995;19:105–25.

[58] Rao PSC, Jawitz JW, Enfield CG, Ronald W. Falta J, Annable MD, Wood AL. Technology integration for contaminated site remediation: clean-up goals and performance criteria, vol. 275. Sheffield, UK: IAHS; 2001.

[59] Rathfelder K, Abriola LM. Mass conservative numerical solutions of the head-based Richards equation. WRR 1994;30:2579–86.

[60] Rathfelder K, Abriola LM. The influence of capillarity in numerical modeling of organic liquid redistribution in two-phase systems. AWR 1998;21:159–70.

[61] Rathfelder KM, Abriola LM, Singletary MA, Pennell KD., The influence of interfacial tension reduction on organic liquid migration: numerical and experimental comparisons Zürich, Switzerland, 1999.

[62] Rathfelder KM, Abriola LM, Taylor TP, Pennell KD. Surfactant enhanced oil recovery of tetrachloroethylene from a porous medium containing low permeability lenses. 2. Numerical simulation. JCH 2001;48:351–74.

[63] Rathfelder KM, Lang JR, Abriola LM. A numerical model (MISER) for the simulation of coupled physical, chemical, and biological processes in soil vapor extraction and bioventing systems. JCH 2000;43:239–70.

[64] Rudin J, Walsh DT. Mechanisms for lowering of interfacial tension in alkali/acidic oil systems. 2. Theoretical studies. J Coll Surf 1992;68:81–94.

[65] Rudin J, Wasan DT. Mechanisms for lowering of interfacial tension in alkali/acidic oil systems. J Coll Surf 1992;68:67–79.

[66] Saenton S, Illangasekare TH, Soga K, Saba TA. Effects of source zone heterogeneity on surfactant-enhanced NAPL dissolution and resulting remediation end-points. J Contam Hydrol 2002;59:27–44.

[67] Sale TC, McWhorter DB. Steady state mass transfer from single-component dense nonaqueous phase liquids in uniform flow fields. WRR 2001;37:393–404.

[68] Schad H. In: Vincenzo C, Giovanni G, Donato P, editors. Statistics of spatial processes: Theory and applications. Italy: Bari; 1993. p. 205–12.

[69] Sudicky EA, Huyakorn PS. Contaminant migration in imperfectly known heterogeneous groundwater systems. Rev Geophys 1991;(supplement):240–53.

[70] Trujillo EM. The static and dynamic interfacial tensions between crude oils and caustic solutions. Soc Petroleum Engr J 1983;23:645–56.

[71] Ustohal P, Stauffer F, Dracos T. Measurement and modeling of hydraulic characteristics of unsaturated porous media with mixed wettability. JCH 1998;33:5–37.

[72] vanGenuchten MT. A closed-form equation for predicting the hydraulic conductivity of unsaturated soils. SSS 1980;44:892–8.

[73] Villaume JF. Investigations at sites contaminated with dense, non-aqueous phase liquids (NAPLs). Ground Water Monitor Rev 1985;10:60–74.

[74] Walser GS, Illangasekare TH, Corey AT. Retention of liquid contaminants in layered soils. JCH 1999;39:91–108.

[75] Wilson JL, Conrad SH, Mason WR, Peplinski W, Hagan E. Laboratory investigation of residual liquid organics from spills, leaks and the disposal of hazardous wastes in groundwater. Environmental Protection Agency; 1990.

[76] Yang J, Zhang R, Wu J, Allen MB. Stochastic analysis of adsorbing solute transport in two-dimensional unsaturated soils. WRR 1996;32:2747–56.

[77] Zheng J, Powers SE. Organic bases in NAPLs and their impact on wettability. JCH 1999;39:161–81.